JJEES
Volume 8, (Number 1), Sept, 2017
ISSN 1995-6681
Pages 27 - 34
Jordan Journal of Earth and Environmental Sciences

Electrical Resistivity Tomography Modeling of Vertical Lithological Contact using Different Electrode Configurations

Hani Al-Amoush[1*], Jafar Abu Rajab[2], Eid Al-Tarazi[2], Abdel Rahman Al-Shabeeb[3], Rida Al-Adamat[3] and A'kif Al-Fugara[4]

[1]Department of Applied Erath and Environmental Sciences, Institute of Earth and Environmental Sciences, Al al-Bayt University, Mafraq, Jordan.
[2]Department of Earth Sciences and Environment, Faculty of Natural Resources and Environmnet, Hashemite University, Zarqa, Jordan
[3]Department of Geographic Information System and Remote Sensing, Institute of Earth and Environmental Sciences, Al al-Bayt University, Mafraq, Jordan
[4]Department of Engineering Survey, Faculty of Engineering, Al al-Bayt University, Mafraq, Jordan

Received 27 May, 2017; Accepted 25 August, 2017

Abstract

In the present study, three different electrical resistivity electrode configurations (Dipole-Dipole, Wenner-Schlumberger, and Wenner configurations) were applied to a geological outcrop that demonstrates a lateral lithological variation at sub-vertical contact. The main target was to examine the intrinsic characteristics of resistivity configurations and consequently to determine the optimum one that has to be selected in such a geological environment. The results of resistivity models provided comparable tomograms at different number of accepted quadripoles and varied RMS%. Based on statistical fitting criteria between four simulated tomograms and three measured inverted tomograms, the inversed twelve data sets produced for three resistivity configurations are capable of defining vertical and horizontal structures with varied sensitivity and fitting values. In particular and according also with known geological outcrop's dimension and lithological layers, Dipole-Dipole resistivity tomogram can be considered as the most sensitive configuration to localized and extended conductive structure at the highest correlation coefficient. On the other hand, Wenner-Schlumberger and Wenner tomograms based configurations can resolve localized horizontal conductive layer beneath resistive layer. In particular, the high resistivity contrast for geoelectrical layers allowed producing similar resistivity tomograms down to 20 m depth.

Keywords: Electrical Resistivity Tomography (ERT), Geological outcrop, Modeling and Inversion.

1. Introduction

Electrical Resistivity Tomography (ERT) has become a powerful method to investigate subsurface shallow structures and geology for various environmental and engineering applications. ERT has been largely used to investigate faulting in shallow subsurface to depths of few tens of meters (e.g., Seminsky et al., 2016; Olenchenko and Kamnev, 2014; Carbonel et al., 2013; Improta et al., 2010; Reiser et al., 2009). In ERT method, the apparent resistivity can be measured by using different electrical configurations. Several electrical configurations have been widely used for various geological applications, e.g., the Schlumberger configuration has been used for Landfill investigation (Monier-Williams et al., 1990) and for hydro-geological purposes (Al-Amoush, 2006). For deep exploration using pole-dipole configuration (Alfano, 1974). The Dipole-Dipole configuration was used for measuring earth conductivity (Alpine et al., 1966). The Gradient configuration was used for veins investigation (Furness, 1993). The Square Array techniques was used for resistivity measurements and fractures distribution (Habberjam, 1979). The Null and Collinear configuration were used to investigate near surface karstic fractures (Szalai et al., 2002; Szalai et al., 2004). The surface and cross-hole resistivity tomography were used to detect foundations of archaeological structures (Tsokas et al., 2011). The Equatorial and Schlumberger configuration were used jointly for groundwater investigation (Zohdy, 1969). Brass et al. (1981) conducted resistivity profiling survey over a graphite deposits utilizing three different electrode arrays (Single pole, Half-Wenner and Half-Schlumberger), the study showed that half-Schlumberger configuration prove to be the most reliable array among others since it shows fine details which were not shown by the other configurations.

A valuable review geophysical study provided a classification of the surface geo-electrical configurations through collecting more than one hundred different independent geoelectric configurations from published geophysical literature (Szalai and Szarka, 2007a; Szalai and Szarka, 2007b). This classification was based on three parameters: superposition of measurements, focusing of currents and co-linearity of configuration producing eight classes of electrical configurations (Szalai and Szarka, 2007a). Wenner and Dipole – Dipole configurations are the most widely used and the others are of less frequently used among possible electrical resistivity configurations (Szalai and Szarka, 2007a). Each of electrical configurations has its advantages and disadvantages in terms of signal strength, vertical / horizontal resolution and data coverage (Table 1)

* Corresponding author. e-mail: hani.alamoush1@gmail.com

(Loke, 2014). Wenner and Wenner-Schlumberger arrays have a moderate depth of investigation and strong signal strength, which permits to be relatively sensitive to vertical variations in the subsurface, but it has less sensitivity to horizontal variations in the substratum. Dipole-Dipole array has better horizontal data coverage but weak signal strength at a greater depth, which makes it the most sensitive to horizontal variations and relatively insensitive to vertical variations of the substratum. A discussion on the properties of different arrays can be found in (Dahlin and Zhou, 2004; Zhou and Dahlin, 2003).

The objective of the present study is to carry out three different electrical resistivity tomography configurations (ERC) over a geological section exhibiting lateral and sharp lithological sub-vertical boundary. The electrical resistivity configurations used in this study are Dipole-Dipole (DD), Wenner-Schlumberger (WS) and Wenner (W) configurations (Figure 1). The choice of ERC configurations was basically built on their wide-varied sensitivity and intrinsic characteristic to geological materials (Table 1). Consequently, to determine the optimum electrical configuration that would be applied in such geological environment. The ERC profiles' azimuth are mainly constrained only to consider the effect of two-dimensional (2D) geological structure, where the lithology is changing abruptly along survey line, and in medium assumed of high- resistivity contrast. Furthermore, statistical investigations are demonstrated at the level of experimental modeled data and for synthetic modeled data. These models data were tested and analyzed for the three ERC models at different geological scenarios. The present study is incorporate a real data measurements and synthetic data modeling collected from Jordan.

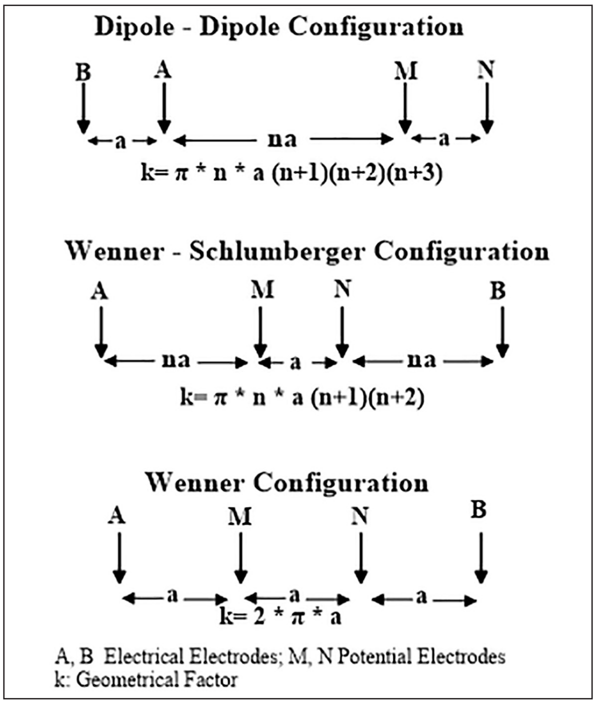

Figure 1. Electrical electrodes configurations used in this study

Table 1. 2D resistivity configurations and survey characteristics, four stars implies the most effective and one star is the least effective (Loke, 2014)

Configuration / Characteristics	Dipole - Dipole (DD)	Wenner - Schlumberger (WS)	Wenner (W)
Sensitivity of the array horizontal structures	*	**	****
Sensitivity of the array vertical structures	****	**	*
Depth of investigation	***	**	*
Horizontal data coverage	***	**	*
Signal Strength	*	***	****

1.1. Description of Study Area

The investigated site is located along Amman - Irbid Highway with coordinates [35.84916º] E, [32.15815º] N according to WGS 1984 coordinate system (Figure 2). The height of the exposure reaches about 14-17m. The site is located at an altitude of 500 masl, and at a distance of 1 km to the south of Philadelphia Private University. The site shows a sharp contact and a pronounced lateral variation in lithology. A nearly sub-vertical contact is cutting the outcrop into two parts. The outcrop consist of two main geological rock types; the northern part consists of a sequence of hard limestone, marly limestone and a weathered top zone, but the southern part of the exposure consists of transported soft sediments and soil material overlying a basal zone of weathered conglomerate and gravel to the lower south (Figure 2).

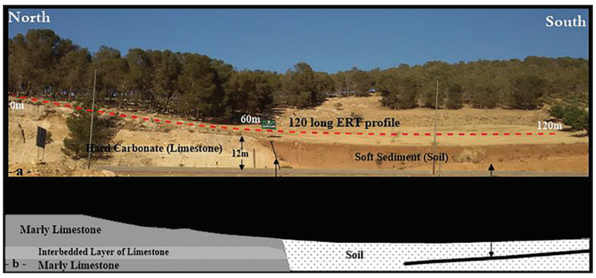

Figure 2. a- Field photo shows an exposure of study site and the extension of ERT survey line, **b-** An illustration of lithological description and the sub-vertical lithological contact. The thick dark black line illustrates the contact between the basal conglomerate, the transported soft sediments and soil material.

2. Materials and Methods

2.1. Survey Design and Instrumentation

In the present study, 2D Electrical resistivity tomography surveys (2D-ERT) were conducted long 120 m, using a multichannel system of 24-electrode with an inter-electrode spacing of 5m, along profile in North- South direction. The designed profile was extended normal to the strike of the fault structure, as shown in Figure (2).

The SYSCAL R-1 resistivity meter (IRIS Instruments, France) was used to survey the area using several electrical resistivity configurations. The multichannel system operates automatically once the type of electrical configuration and geometrical parameters are defined. The system has an internal microprocessor controlled together with electronic automatic switching unit used to recording independently a hundred of resistivity data (Loke, 2014). Electrical resistivity tomography is usually performed using 24-electrode or more, connected together with a multi-core cable (Griffiths and Barker, 1993; Reynolds, 2011). After instrumentation and field setup, resistivity measurements are automatically recorded and saved in resistivity meter system.

The sequence of measurements, such as type of configuration, survey parameter and electric current duration, can be set manually at the field or prepared preliminary and transferred to microprocessor of the system using laptop. The 2D electrical resistivity tomography survey was carried out using Wenner, Dipole-Dipole and Wenner-Schlumberger configurations. ELECTRE PRO software was used to create the measurements sequence, and PROSYS II was used to download, edit and filter the stored data after field survey completion.

2.2 Data Quality and Error Sources

Resistivity measurements are routinely subjected to systematic errors resulting from insufficient current injection due to the high electrode-ground contact resistance. Further minor effects are commonly resulted from different sources, e.g., electrode polarization and position, inductive and capacitive coupling of wired system of instrument, and external low frequency currents effects (Zhou and Dahlin, 2003; Dahlin and Leroux, 2012).

The presentation of resistivity pseudo-sections of three different configurations enables to investigate the noise of each data level (quadripoles datum). SYSCAL R-1 resistivity-meter introduces a quality factor that based on the estimated Standard Deviation (SD) (i.e., known also as the repeatability error). The instrument calculates the resistance (R=V/I) for each datum up to six stacking. In the present study, the standard deviation of the (V/I) ratio was set to be less than 5% at two seconds current pulse length. The presented pseudo-sections for three configurations showed unsystematic character for resistivity data level at poorly performing electrodes. Many of noisy data were associated with the threshold value of received voltage Vp (< 5 mV) (Table 2). Generally, we rejected data and determined the cut off margin of at which SD is more than 5%. Nevertheless, the vast majority of stacking errors have reached 1% of their SD value (see average SD in Table 2).

Table 2 lists the statistical summary of the processed measured parameters for three ERC profiles, including the accepted and rejected quadripoles and their statistical annotations; maximum, minimum, mean, and standard deviation values for different acquiring parameters.

Table 2. Statistical summary of the processed measured parameters for three resistivity configurations

Noise %	Quadripole (accepted/ acquired)	Average Standard deviation (quality factor, in %)	Vp (mV) (Min/Max)	Average measured primary voltage Vp (mV):	Average Injected current intensity (mA)	Average Injected voltage (V)	Average grounding resistance value of the injection dipole (in kOhm)	Resistivity Configuration
5.8	195/207	0.6	92/575	98	148.2	371.9	16.4	Dipole-Dipole (DD)
28.3	367/512	0.8	17/23.6	11	20.6	202.1	28.1	Wenner-Sclumberger (WS)
5	76/84	0.6	6/18	12.1	17.9	202.0	31.8	Wenner Array (W)

2.3. Forward Modeling and Inversion

In designing Electrical Resistivity Tomography survey line, forward modeling is commonly used to investigate the possibility of creating ground resistivity models such that the measured ERT data can be better interpreted and explained prior inversion procedure. According to Dey and Morrison (1979), the measured or simulated electrical potential divided by applying electrical current provided between pairs of electrodes allow to calculate resistivity values at different datum based on equation (1):

$$\nabla \cdot \sigma \nabla \phi = I\,\delta(x - xs, y - ys, z - zs \qquad (1)$$

where

σ is the electrical conductivity, an intrinsic property of the material;

φ is the electrical potential;

I is the electrical current source;

δ is the Dirac delta function;

x ,y, z are the spatial position vectors; and

xs, ys, zs are the spatial coordinates of the current source.

The modeling procedure of 2D resistivity measurements is commonly solved based on Finite-Difference (FD) or Finite-Element (FE) solution of the electrical resistivity. In the present study, a forward modeling calculation implemented by RES2DMOD software (Loke, 2014) using the Finite-Element (FE) mesh method in order to calculate the two-dimensional resistivity distribution. The measured data for the three conducted ERT profiles anticipated to create four synthetic models using three different configurations (Figure 1) and provide insight into the possibility of resolving power of different survey geometries at different geological structures.

The resistivity data are inverted to create a model section of the area under the investigated ERT line. Owing to resistivity distribution of three conducted data sets, the resis¬tivity inversion procedure entails the Robust Data Constraint (L1-norm), which is commonly applied to emphasize the boundary between soil and the bedrock or vertical fault contacts. In addition, it is used to minimize the effect of outliers in the data (Loke, 2014). The inversion problem is solved to determine the resistivity of the discretised cells that will minimize the difference between calculated and measured apparent resistivity values (Loke et al., 2003). Applying the inversion setting to observed data requires the use of regularization to solve the non-linear inversion problem and to produce a stable solution for the ill-posed problem. Therefore, the measured ERT sections are processed and inverted to produce a unique smooth model with proper resolution according to the optimization equation proposed by Loke (2014):

$$(\mathbf{J^T J} + \lambda \mathbf{F_R})\Delta \mathbf{q_K} = \mathbf{J^T R_d g} - \lambda \mathbf{F_R}\, \mathbf{q_K} \quad \text{.............................(2)}$$

with $\mathbf{F_R} = \alpha_x \mathbf{C_x^T R_m C_x} + \alpha_z \mathbf{C_z^T R_m C_z}$,

$\Delta \mathbf{q_K}$ represents the change in the i-th model response due to changes in the j-th model parameter, is the Jacobian matrix (of size m×n) of partial derivatives, and is the transpose of .The factor represents the damping factor, g is the discrepancy vector between the observed data and the model response (i.e., the data misfit error), and Rd and Rm are the weighting matrices introduced so that different elements of the data misfit and model roughness vectors are given equal weight in the inversion process (Loke, 2014). Cx and Cz are the smoothing matrices in the x- and z-directions, respectively, and αx and αz are the relative weights given to the smoothness filters in the x- and z-directions, respectively (Loke, 2014).

The resistivity pseudo-sections for measured and synthetic data were inverted using the RES2DINV software package (Loke, 2014). The inversion parameters were unified and implemented for the three ERT's configurations.

For quantitative comparison criteria, a statistically-based procedure was performed between inverted resistivity data and inverted synthetic resistivity data for the four proposed models of each ERT configuration. The statistical procedure implemented in the present study is a direct link between real resistivity model parameters (inverted resistivity, cell coordinates: Xi and Zi) with synthetic model parameters (synthetic resistivity, cell coordinates: Xi and Zi). So that both models parameters are fixed in model space. The regression line defines the degree of closeness between model parameters. In order to make cross plot fitting and for the reason that the RES2DINV and RES2MOD codes are two independent programs: a quantitative comparisons can be implemented by adjusting the thicknesses of known electrical layers for the measured and synthetic data cells such that they exist in the same location and their corresponding boundaries; this procedure implies that the discretised cells from both models must coincide with the positions of the electrodes.

2.4 Sensitivity Analysis and Inversion Resolution

To gain insight into the reliability and resolving quality of the ERT tomograms in terms of their investigative depth and inversion criteria, the Res2dinv package (Loke, 2010) is used to calculate a models' resolution and sensitivity matrices (Friedel, 2003). During the inversion process of each ERT line, both resolution and sensitivity matrices are computed; the resolution scale can be used to directly indicate the presence of possible artifacts in electrical structures and used to define the depth below which electrical structures do not depend on the measured data but rather result from a poorly resolved inversion process. Moreover, the sensitivity scale achieve semi- quantitative insight into how resolution varies spatially over a tomogram; a cell of high sensitivity values are relatively well constrained by the measured data, whereas low values indicate poorly performing measured data (Oldenburg and Li, 1999).

In the study area, the sensitivity values located in the range between 0.05 to about 2.5 for the domain of three sensitivity tomograms. According to our study area, the outcrop's depth is about 12-15 m, where the resolution value of 0.24 apparently coincides with the depth ranges from 10 to 13 m for W and WS models (Figures 4 and 5). Hence, the value of 0.24 is the line apparently separates poorly performing quadripoles from well-performing quadripoles (i.e., many of rejected quadripoles located below this line). However, the 0.24 resolution line in the DD model denotes a higher depth to about 19 m and it was limited to the north direction of the tomogram (Figure 3). Thus, we consider this resolution line as a reliable depth limit to interpret resistivity structures.

3. Results and Interpretation

The inverted ERT models of three ERT lines converged after seven iterations and yielded root mean square error (RMSE in %) or misfit values for resistivity that are varied with respect to the survey data error (i.e., 5%). Dipole-Dipole resistivity tomogram presented the highest error (13.4%) (Figure 3), whereas the RMSE for Wenner-Schlumberger and Wenner configurations was found to be below 5% (Figures 4 and 5, respectively). In order to make visual comparison among different resistivity tomograms, the resistivity distribution of measured, calculated and inverted data were displayed using a fixed and unified resistivity scale and applied to all resistivity tomograms. Hence, we present the term "resistivity tomogram" to describe the final inversion resistivity model for measured or synthetic data sets.

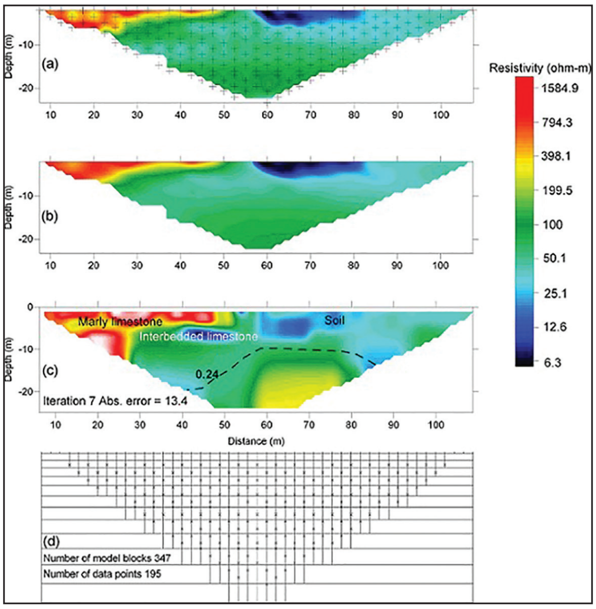

Figure 3. Electrical resistivity model of the Robust inversion using Dipole - Dipole configuration; **(a)** Measured apparent resistivity (pseudo-section) tomogram, **(b)** Calculated resistivity tomogram, and **(c)** The inversion model converged at RMS% = 13.4. Dashed line indicates model sensitivity value, and **(d)** Arrangements of model blocks and resistivity data points.

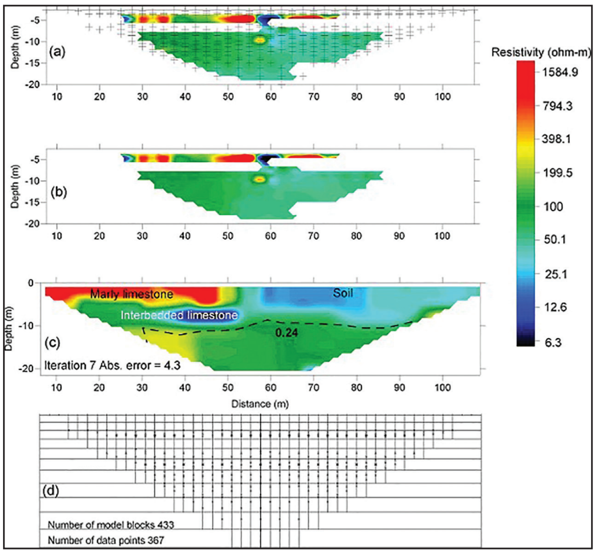

Figure 4. Electrical resistivity model of the robust inversion using Wenner-Schlumberger (WS) configuration; **(a)** measured apparent resistivity (pseudo-section) tomogram, **(b)** calculated resistivity tomogram, **(c)** The inversion model converged at RMS% = 4.3. Dashed line indicates model sensitivity value, and **(d)** Arrangements of model blocks and resistivity data points.

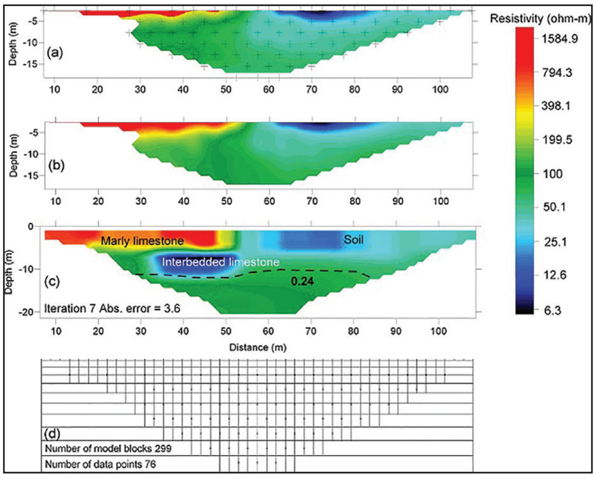

Figure 5. Electrical resistivity model of the robust inversion using Wenner (W) configuration; **(a)** Measured apparent resistivity (pseudo-section) tomogram, **(b)** Calculated resistivity tomogram, **(c)** The inversion model converged at RMS% = 3.6. Dashed line indicates model sensitivity value, and **(d)** Arrangements of model blocks and resistivity data points.

All resistivity tomograms resolved earth's structure down to a depth of 20 m, which exceed outcrop's depth dimension. The number of data points below 0.24 resolution line are varied, and mainly dependent on resistivity configurations (Figures 3, 4, 5; Table 1), however, a 20 m depth seems to be consistent, as all recovered models have approached this range.

The field investigation of the site (Figure 2) shows lateral variation between hard carbonate rock and soft sediments where the sub-vertical sharp contact outlines the boundary between two types of lithology down to 10m depth. The pseudo-sections obtained by (DD) (Figure 3a) and (W) (Figure 5a) demonstrated certain resistivity variation at horizontal distance located between 40 to 60 m, but the (WS) pseudo-section (Figure 4a) did not recognize this anomaly due to many rejected quadripoles at shallow datum (Table 2). As a result, the three resistivity tomograms revealed three resistivity blocks as; hard carbonate layer (~2000 ohm-m), soft sediment (soil) layer (~20 ohm-m) and an unknown (unexposed) layer of 200 ohm-m (Figures 3c, 4c, and 5c).

Additionally, the three resistivity tomograms confirmed the development of a conductive layer of ~10 ohm-m at a depth less than 10 m located below the resistive hard carbonate (limestone) rock. Furthermore, the resistivity contrast across sharp contact has changed and became unclear at the depth located between 6 to 20 m in all resistivity tomogram.

The presented inversion outcomes provide three anomalies that need to be inspected using forward modeling, first, the existence of such conductive layer of ~20 ohm-m at two-setting (i.e., localized or extended horizontal feature), second, the presence of moderate resistivity layer of 200 ohm-m (i.e., extended horizontal feature), third, the continuation of sharp contact down to the tomograms' depth at two-setting (i.e., localized or extended vertical feature).

Therefore, it was possible to develop four synthetic models encompass the possibility to answer the aforementioned cases. Figures 6, 7, 8, and 9 use the measured ERT lines' design in term of electrode spacing, separation, and length. In addition, all synthetic models were included by the domain of two to three resistivity values, such as 20, 200, and 2000 ohm-m, which are related to soft sediment, unexposed layer, and exposed hard rock, respectively. Each synthetic model produces resistivity data for the three applied configurations (i.e., DD, WS, and W), and inverted by applying inversion parameters similar to those used for inversion of measured data. Moreover, each synthetic data set was incorporated by adding 5% Gaussian error. This error value coincides roughly with the error obtained from the associated errors propagated into measured resistivity values (Table 2).

The results of twelve resistivity tomograms rendered resistivity distribution in the domain of measured resistivity scale (see resistivity scale for Figures 3, 4, and 5). This implies that the presentation of resistivity variations by two to three resistivity layers as 20 ohm-m, 200 ohm-m, and 2000 ohm-m is adequate to describe the possible and varied geological setting of the area under investigation.

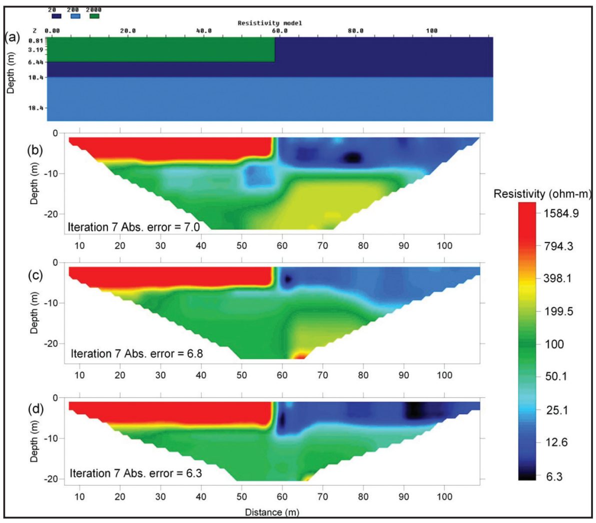

Figure 6. **(a)** Synthetic model simulating MODEL1 structure based on reference of three –resistivity blocks; conductive layer of ~20 ohm-m at extended horizontal feature. **(b)** Inverted forward model of Dipole-Dipole data. **(c)** Inverted forward model of Wenner-Schlumberger data **(d)** Inverted forward model of Wenner data.

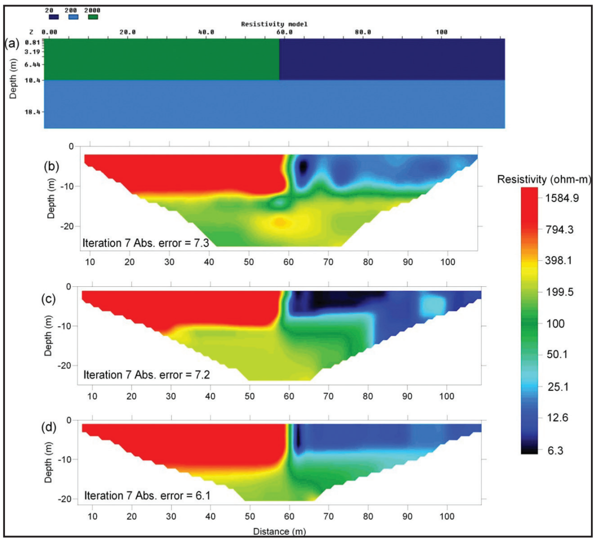

Figure 7. **(a)** Synthetic model simulating MODEL2 structure based on reference of three –resistivity blocks; moderate resistivity layer of 200 ohm-m of extended horizontal feature and localized sharp contact. **(b)** Inverted forward model of Dipole-Dipole data. **(c)** Inverted forward model of Wenner-Schlumberger data **(d)** Inverted forward model of Wenner data.

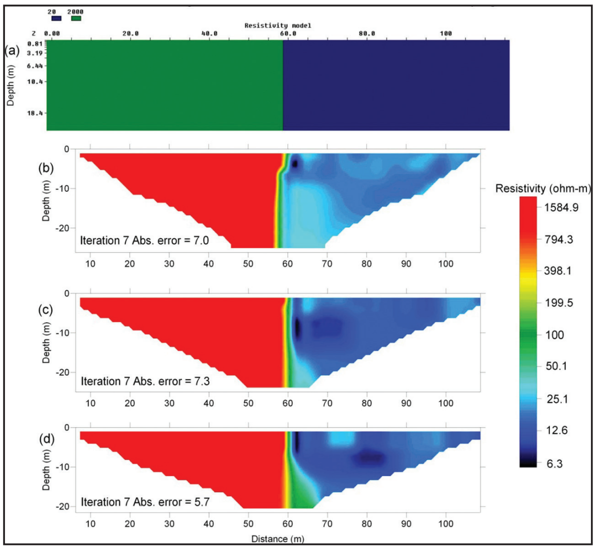

Figure 8. **(a)** Synthetic model simulating MODEL3 structure based on reference of two–resistivity blocks; sharp contact of extended vertical feature. **(b)** Inverted forward model of Dipole-Dipole data. **(c)** Inverted forward model of Wenner-Schlumberger data **(d)** Inverted forward model of Wenner data.

4. Discussion

The present case study performed shallow resistivity imaging using three different resistivity configurations (DD, WS, and W) applied across an outcrop of 10-15 m thickness at road cut exposure. The geological outcrop consists of sharp sub-vertical contact located between the left-hand exposure composed of hard rocks of limestone and marly limestone and the right-hand exposure composed of soil intercalating with a thin zone of conglomerate and gravel.

The three ERC data sets were classified on the basis of the number of data measurements or quadripoles. The classes revealed three categories as low (W), intermediate (DD), and high (WS) (Tables 1 and 2).

The resistivity models have converged at survey data error (i.e., <5%) particularly for (WS) and (W), and reached

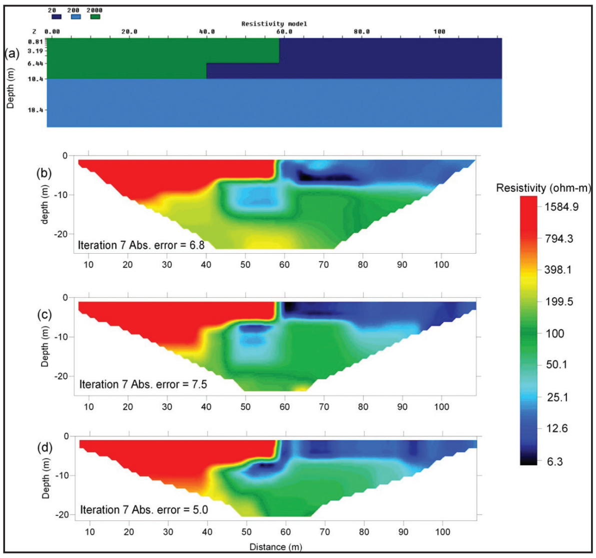

Figure 9. **(a)** Synthetic model simulating MODEL4 structure based on three reference resistivity; conductive layer of ~20 ohm-m at localized horizontal feature. **(b)** Inverted forward model of Dipole-Dipole data. **(c)** Inverted forward model of Wenner-Schlumberger data **(d)** Inverted forward model of Wenner data.

to about 13.4% for (DD). It should be mentioned here that the high-density data related to near surface quadripoles obtained by (WS) configuration (Figure 3 and Table 2) are mainly attributed to poor performing electrodes due to high resistance of ground surface. Despite the high noisy data involved in (WS) configuration, but the final resistivity model can be comparable to other models. Consequently, the results of inversion show correlated resistivity models although they have different numbers of accepted/rejected quadripoles and varied RMS % (Figures 3, 4, and 5).

In order to test the results at different scenarios recommended for this case study, the pseudo-resistivity section of each ERC allowed to build four electrical models based on resistivity distributions with respect to known geological materials (i.e., up to three resistivity zones), resistivity variations (i.e., 5-2000 ohm-m), and model resolution (i.e., down to 20 m depth). Thus, the modeling procedure permitted to create and synthesize four possible geoelectrical signatures. For example, in Model (1) and Model (4) where the forward modeling tests incorporated a conductive layer (20 ohm-m) (see Figure 6 for interbedded layer of limestone) embedded between the resistive sequences. The conductive layers was treated as an extended and as a localized layer model, respectively (see Figures 6 and 9, respectively). Moreover, Model (2) shows extended horizontal layer of moderate resistivity (200 ohm-m) overlain by two layers demonstrate lateral variation (Figure 7), and Model (3) shows sharp contact of extended vertical feature between two layers of high resistivity (2000 ohm-m) and low resistivity (20 ohm-m) (Figure 8).

The resistivity models obtained from measured and synthetic data sets show that all arrays are capable of defining vertical and horizontal structures with varied sensitivity in vertical and horizontal dimensions. For instance, Model 1 and Model 4 reveal that (DD) configuration is almost more sensitive to localized and extended conductive structure (Figures 6b, 9b). On the other hand, (WS) and (W) configurations can resolve horizontal conductive layer beneath resistive layer at localized area (Figures 6c, 6d; 9c, 9d). Figures 7 and 8, Model 2 and Model 3, respectively, show similar horizontal and vertical sensitivity presented for the three configurations assuming simple near surface lateral variation and involving limited vertical structure and lateral variation, built at extended vertical structure. Accordingly, based on forward and inverse models, the variation in configurations' sensitivity demonstrated in Table (1) can be slightly ignored. The slight variation in configurations' sensitivity can be distinguished in this study where the geoelectrical layers show a strong resistivity contrast, the procedure of filtering noisy quadripoles, and the choice of inversion method and its parameters. For instance, 100 times resistivity difference from the low resistivity layer (10-20 ohm-m) to the highest resistivity layer (2000 ohm-m) is adequate to sharply image near surface geoelectrical structures in proper details. This can be concluded from the localized conductive structure presented in Figure 9. However, we propose that the variations of configurations' characteristics (Table 1) could be triggered at least in such environment characterized by low resistivity contrast. This could tested numerically using variable electrodes' spacing and configurations applied for similar case studies, where the target is placed at greater depth, and this was beyond the objective and field design of this study.

In order to give quantitative comparisons between real earth tomograms and the synthetic tomograms, each measured tomogram was quantitatively connected and correlated to the four synthetic tomograms. The fitting criteria results entail statistically significant variation using R-squared values (i.e., correlation coefficient). Figures 10, 11, and 12 compare resistivity values at datums of equal depths and spacing among the four synthetic tomograms presented in Figures 6, 7, 8, and 9.

In order to improve data display, we used logarithmic scale axis and applied the logarithmic value "Log10" of resistivity for measured and synthetic models. At this point, the fitting line established the degree of misfit (closeness) between the measured and modeled data for the whole data set. The three resistivity configurations are considered to be moderately resolved (i.e., R2 > 50 %), such as the measured tomogram and synthetic tomogram are probably fit Model 1 and Model 4 (Figures 6 and 9). In addition, the fitting plot parameters for Model 4 revealed the highest correlation (i.e., R2 ~ 70%) and has fairly resolved the existence of localized conductive layer (i.e., interbedded limestone) at the contact between hard rock and soft sediment at depth of 6 m (Figure 2). Furthermore, it confirms the limited extent of near surface sharp contact, and also provided the existence of resistive marly limestone layer at depth of 10 m down to resistivity tomogram's depth (see Figure 9, and model 4 data in Figures 10, 11, and 12).

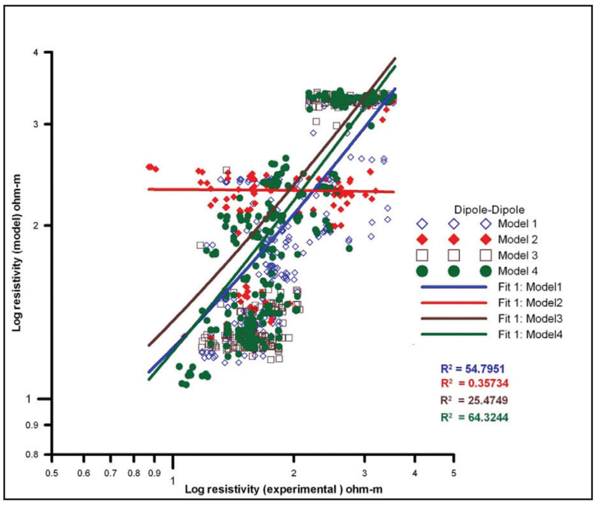

Figure 10. Statistical analysis and fitting parameter between measured (Dipole-Dipole) and four resistivity models

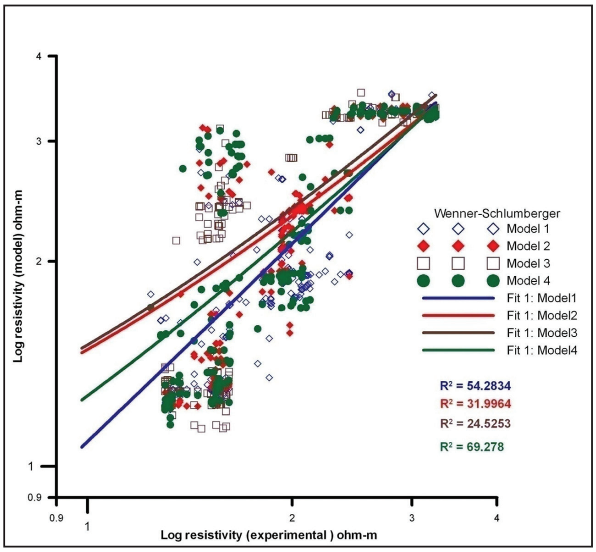

Figure 11. Statistical analysis and fitting parameter between measured (Wenner-Schlumberger) and four resistivity models

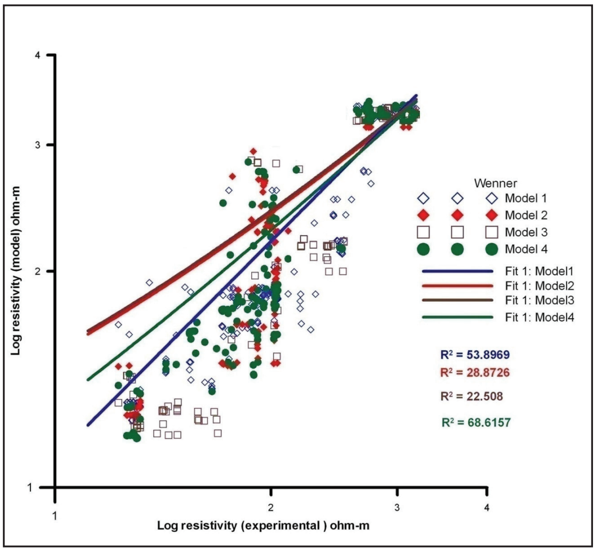

Figure 12. Statistical analysis and fitting parameter between measured (Wenner) and four resistivity models.

Conclusions

Experimental and synthetic electrical resistivity tomography were used to study lithological variation at geological outcrop area. The sequence of hard rocks of limestone, marly limestone, and soil have posed several geoelectrical signatures on resistivity tomograms. Three resistivity configurations (ERC) including Wenner-Sclumberger (WS), Dipole-Dipole (DD), and Wenner (D) have yielded a varied number of data measurements and classified as low, intermediate, and high, respectively.

The results of three resistivity tomograms provided similar geoelectrical structures and can be correlated to real earth model. All models show similar sensitivity to high and low resistivity layers and can be effectively resolve resistivity variations at different degree of data noises. The DD and W configurations seem to be less contaminated by noise levels comparable to Wenner–Schlumberger (WS) configuration. Besides, many of rejected near surface noisy data observed in WS pseudo-section do not have fundamental influence to resolve resistivity structures at greater depth. Moreover, the present study, where the depth of investigation is 20 m and the medium resistivity contrast, is relatively high for the different embedded structures; the applied ERCs have recovered real earth resistivity models at fine details where it was not compulsory to acquire large number of measurements.

The synthetic resistivity models allowed producing four geoelectrical scenarios to imitate possible geological structures. The resolution of DD configuration appears to be more effective at larger depth than WS and W configurations, and exhibited a model of quite more sensitive to small and localized conductive layer at shallow depth.

References

[1] Al-Amoush, H. R. 2006. Hydro-Geophysical Investigations for the Purposes of Groundwater Artificial Recharge in the Jordan Valley Area, Ph.D. Dissertation, University of Jordan, Amman.

[2] Alfano, L., 1974. A modified geoelectrical procedure using polar-dipole array – An example of application to deep exploration, Geophysical prospecting, 22: 510-525.

[3] Alpine L.M, Berdichevsky, M.N., Vedriintsev, G.V and Zagramister, A.M., 1966. Dipole methods for measuring earth conductivity (selected and translated from russion by G.V Keller). Colorado School of Mines, Golden co.

[4] Brass, G., Flathe, H., and Schulz, R., 1981. Resistivity Profiling with Different Electrode Arrays over a graphite deposits, Geophysical Prospecting, 29: 289-600.

[5] Carbonel, D., Gutiérrez, F., Linares, R., Roqué, C., Zarroca, M., McCalpin, J., Guerrero, J., and Rodríguez, V., 2013. Differentiating between gravitational and tectonic faults by means of geomorphological mapping, trenching and geophysical surveys. The case of the Zenzano Fault (Iberian Chain, N Spain), Geomorphology 189: 93–108.

[6] Dahlin, T., and Leroux, V., 2012. Improvement in time-domain induced polarization data quality with multi-electrode systems by separating current and potential cables, Near Surface Geophysics 10: 545-656.

[7] Dahlin, T., and Zhou, B., 2004. A numerical comparison of 2D resistivity imaging with 10 electrode arrays, Geophysical Prospecting, 52: 379-398.

[8] Dey, A., and Morrison, H.F., 1979. Resistivity modeling of arbitrary shaped two-dimensional structures, Geophysical Prospecting, 27: 106-136.

[9] Friedel, S., 2003. Resolution, stability and effciency of resistivity tomography estimated from a generalized inverse approach, Geophys. J. Int, 153: 305–316.

[10] Furness, P., 1993. Gradient Array profiles over thin sensitive veins, Geophysical prospecting, 41: 113-130.

[11] Habberjam, G.M., 1979. Apparent resistivity observations and the use of square Array Techniques. In Saxov, S and H. Flathe (eds), Geoexploration Monographs, series 1, (9), pp.1-152. Geopublication Associates, Gebruder Borntraeger.

[12] Improta, L., Ferranti, L., De Martini, P.M., Piscitelli, S., Bruno, P.P., Burrato, P., Civico, R., Giocoli, A., Iorio, M., D'Addezio, G.,and Maschio, L., 2010. Detecting young, slow-slipping active faults by geologic and multidisciplinary high-resolution geophysical investigations: A case study from the Apennine seismic belt, Italy. J. Geophys. Res. 115, B11307. doi:10.1029/2010JB000871.

[13] Griffith, D. H., and Barker R.D., 1993. Two-dimensional resistivity imaging and modeling in areas of complex geology, Journal of Applied Geophysics, 29: 211-226.

Loke, M. H., 2010. Tutorial: RES2DINV version 3.59, Rapid 2-D Resistivity & IP Inversion Using the Least-Squares Method Malaysia. Geotomo Software.

[14] Loke, M.H., 2014. Tutorial: 2-D and 3-D electrical Imaging Surveys, Malaysia. Geotomo Software.

[15] Loke, M. H, Acworth, I., and Dahlin, T., 2003. A comparison of smooth and blocky inversion methods in 2D electrical imaging surveys, Exploration Geophysics, 34: 182-187.

[16] Monier-Williams, M.E., Greenhouse, J.P., Mendes, J.M. and Ellert, N., 1990. Terrain conductivity mapping with topographic corrections at three waste disposal sites in Brazil, in Geotechnical and Environmental Geophysics, Vol. 2: Environmental and Groundwater (ed. S.H. Ward), Society of Exploration Geophysicists, Tulsa, Oklahoma, USA, pp. 41–55.

[17] Olenchenko, V.V., and Kamnev, Ya .K., 2014. A resistivity model of permafrost in the Zhosaly Kezen Pass (Ilei Alatau), from ERT data, in: Proc. Geo-Siberia Int. Conf. & Expo, Vol. 2 (2): 1–5.

[18] Oldenburg, D.W. and Li. Y., 1999. Estimating the depth of investigation in dc resistivity and IP surveys, Geophysics 64: 403–416.

[19] Reiser, F., Dalsegg, E., Dahlin, T., Ganerod, G.V., and Ronning, J.S., 2009. Resistivity modeling of fracture zones and horizontal layers in bedrock, Geol. Survey Norway, Report No. 2009.070, pp.1-120.

[20] Reynold, M. J., 2011. An Introduction to Applied and Environmental Geophysics, 2nd edn., Wiely Blackwell, UK. 696p.

[21] Seminsky, K., Zaripov, R. and Olenchenko, V., 2016. Interpretation of shallow electrical resistivity images of faults: tectonophysical approach, Russian Geology and Geophysics 57: 1349–1358.

[22] Szalai, S., Szarka, L., 2007b. Auxiliary Results of Collection and Classification of Surface Geoelectric Arrays, 13th European

[23] Meeting of Environmental and Engineering Geophysics, Istanbul A09.

[24] Szalai, S., and Szarka, L. 2007a. On the classification of surface geoelectrical arrays, Geophysical Prospecting, 56: 159-175.

[25] Szalai, S., Szarka, L., Praceser, E., Bosch, F., Muller, I. and Turberg, P., 2002. Geoelectrical mapping of near-surface karstic fractures by using null arrays, Geophysics 67: 1769-1778.

[26] Szalai, S., Szarka, L., Marquis, G., Sailhac, P., Kakkonen, P. and Lahti, I., 2004. Colinear null arrays in geoelectrics. Proceeding of the 17th workshop on electromagnetic induction in the earth, S.3-P3 IAGA WG 1.2 , Hyderabad, India.

[27] Tsokas, G.N., Tsourlos, P.I., Vargemezis, G.N., and Pazaras, N.T., 2011. Using surface and cross-hole resistivity tomography in an urban environment: an example of imaging the foundations of the ancient wall in Thessaloniki, North Greece, Physics and Chemistry of the Earth, 36 (16): 1310–1317.

[28] Zhou, B, and Dahlin, T., 2003. Properties of effects of measurements errors on 2D resistivity imaging, Near Surface Geophysics, 1: 105-117.

[29] Zohdy, A., 1969. The use of Schlumberger and equatorial soundings in groundwater investigations near El Paso, Texas, Geophysics 34: 713-728.